

Effect of chain length and asymmetry on material properties of bilayer membranes

G. Illya,^{a)} R. Lipowsky, and J. C. Shillcock

Max Planck Institute of Colloids and Interfaces, D-14424 Potsdam, Germany

(Received 14 January 2005; accepted 25 March 2005)

Dissipative particle dynamics is used to extract the material parameters (bending and area stretch moduli) of a bilayer membrane patch. Some experiments indicate that the area stretch modulus of lipid vesicles varies little as the chain length of the lipids composing the bilayer increases. Here we show that making the interactions between the hydrophilic head groups of the model amphiphiles proportional to the hydrophobic tail length reproduces the above result for the area stretch modulus. We also show that the area stretch modulus of bilayers composed of amphiphiles with the same number of tail beads but with asymmetric chains is less than that of bilayers with symmetric chains. The effects on the bilayer density and lateral stress profiles of changes to the amphiphile architecture are also presented. © 2005 American Institute of Physics. [DOI: 10.1063/1.1917794]

I. INTRODUCTION

The dependence of the material properties of lipid bilayer membranes on the structure of their component molecules is important biologically and commercially. The plasma membrane that surrounds all living cells must be strong enough to prevent the permeation of unwanted ions and molecules, but also flexible enough so that, for example, red blood cells can squeeze through capillaries whose width is only one-third of the cell's diameter.¹ Commercially, artificial lipid vesicles are potential vehicles for drug delivery systems.² The lifetime of the drug-filled vesicles in the bloodstream is dependent on the robustness of the membrane, and limits how long the drug can be encapsulated. Experiments³ have found that the resistance of lipid vesicles to electric-field-induced rupture depends on the type of lipid and on the presence or absence of cholesterol. Lipids with a high degree of unsaturation in their hydrocarbon tails have been found to reduce the bending rigidity of a vesicle by a factor of two compared to their saturated counterparts, while leaving the membrane's area stretch modulus approximately unchanged.⁴ Monolayers of lipids with asymmetric chains are also found to be less rigid than those composed of lipids with equal length tails.⁵

In the pursuit of a quantitative understanding of the influence of molecular architecture on the properties of membranes, computer simulations have been a valuable tool. Molecular-dynamics (MD) simulations⁶ have been used for many years to study the properties and behavior of small molecules, but are typically limited to a few hundred molecules,⁷ plus solvent particles; although simulations of 1024 dipalmitoylphosphatidylcholine lipids in a 20-nm square patch have recently been performed⁸ that required 30 000 CPUh. Coarse-grained MD has been developed to measure the properties of larger systems for longer times by combining several atomic groups into one coarse-grained

particle. In this way, a typical lipid molecule that contains more than 100 at. can be represented by approximately 10–15 coarse-grained particles. This procedure retains enough detail to capture the essential differences between various chemical species,^{9–12} and has been shown capable of following the fusion of small vesicles.¹³ Because even coarse-grained MD requires large amounts of computer time to simulate sizable membrane patches, a new particle-based, mesoscopic simulation technique developed in the 1990s has recently been applied to the problem of simulating large membrane patches. Dissipative particle dynamics (DPD) was introduced in 1992 by Hoogerbrugge and Koelman, who applied it to measuring the hydrodynamic drag on a cylinder in a moving fluid.¹⁴ The algorithm was modified by Groot and Warren and used to study the phase separation of immiscible polymeric fluids.¹⁵ Their scheme has since been used to investigate pore formation in amphiphilic bilayers,¹⁶ to follow the self-assembly of vesicles,¹⁷ phase separation in vesicles,¹⁸ and vesicle budding;¹⁹ to calculate the material properties of single-component membranes;²⁰ and to explore the phase behavior of lipids²¹ and the effects of surfactant packing at an oil-water interface.²²

Here we use the DPD simulation technique to explore the dependence of the area stretch modulus and corresponding bending rigidity of a planar membrane patch on its component lipid architecture. We find that the experimental result of the independence of the membrane area stretch modulus on tail length⁴ is reproduced in the simulations if the polar head group's interactions are correlated with the tail length. We also show that model lipids with mismatched tail lengths form bilayers whose stiffness is much reduced compared to that of bilayers composed of symmetric tail lipids, a result also found in experimental work.⁵ Such asymmetric amphiphiles also redistribute the lateral stresses in the membrane, a process that has been suggested as important for the functioning of anaesthetics.²³

^{a)}Electronic mail: illya@mpikg-golm.mpg.de

II. DISSIPATIVE PARTICLE DYNAMICS SIMULATION METHOD

In the dissipative particle dynamics method, the molecules of a fluid are grouped together to form fluid elements, or beads that interact via soft, short-range forces. Each bead has a mass m_0 and diameter d_0 , and the average density of the system is constant. The bead coordinates evolve in time under their mutual interactions according to Newton's laws of motion. Each bead experiences three forces with those of its neighbors within the range d_0 . The conservative force takes the form

$$\mathbf{F}_{ij}^C = a_{ij}(1 - r_{ij}/d_0)\hat{\mathbf{r}}_{ij}, \quad (2.1)$$

for $r_{ij} < d_0$, and zero otherwise. Here a_{ij} is the maximum repulsion between bead types i and j which are separated by a distance of r_{ij} , and $\hat{\mathbf{r}}_{ij}$ is the unit vector pointing from bead j to bead i . This force gives beads an identity that governs their compressibility and mutual miscibility. Additionally, dissipative and random forces are used to apply a thermostat to the system that ensures it evolves towards a Boltzmann-distributed equilibrium state. The two forces are related to one another by fluctuation-dissipation theorem, i.e., the temperature is a result of the balance between the noise and friction strengths.

The dissipative force is of the form

$$\mathbf{F}_{ij}^D = -\gamma_{ij}(1 - r_{ij}/d_0)^2(\hat{\mathbf{r}}_{ij} \cdot \mathbf{v}_{ij})\hat{\mathbf{r}}_{ij}, \quad (2.2)$$

for $r_{ij} < d_0$, and zero otherwise, where γ_{ij} and \mathbf{v}_{ij} are the dissipation strength and relative velocity between beads i and j , respectively.

Finally, the random force is

$$\mathbf{F}_{ij}^R = \sqrt{2\gamma_{ij}k_B T}(1 - r_{ij}/d_0)\zeta_{ij}\hat{\mathbf{r}}_{ij}, \quad (2.3)$$

for $r_{ij} < d_0$, and is pairwise symmetric for all pairs of interacting beads. Here, ζ_{ij} is a uniform random variable that satisfies $\langle \zeta_{ij}(t) \rangle = 0$ and $\langle \zeta_{ij}(t)\zeta_{i'j'}(t') \rangle = (\delta_{ii'}\delta_{jj'} + \delta_{ij'}\delta_{ji'})\delta(t - t')$.

Because all three of these forces conserve momentum locally, hydrodynamic behavior emerges even in systems containing only a few hundred particles.¹⁴

Beads are assembled into amphiphilic molecules by tying them together with Hookean springs with the potential

$$U_2(i, i+1) = 1/2k_2(|\hat{\mathbf{r}}_{i,i+1}| - l_0)^2, \quad (2.4)$$

where the spring constant and unstretched bond length may be determined by comparing the end-to-end length of the model amphiphile with the actual molecular length.

In order to represent the noninterdigitated state of typical lipid bilayers, it has been found necessary to add a chain stiffness potential to the amphiphiles' tails, U_3 , where

$$U_3(i-1, i, i+1) = k_3[1 - \cos(\theta - \theta_0)], \quad (2.5)$$

in which the bending stiffness and preferred angle are chosen so as to produce a stable bilayer.^{11,20}

We consider amphiphiles with symmetric and asymmetric tails, which we model using the general architectures $H_m(T_{n_1})_2$ and $H_m T_{n_1} T_{n_2}$, respectively, where n_1 and n_2 are the number of hydrophobic beads in each tail and the head group

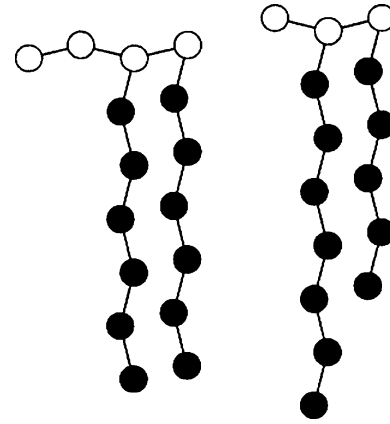


FIG. 1. Illustration of the amphiphile architectures used in the simulations, $H_4(T_6)_2$ and $H_3T_7T_5$. The polar head beads are connected linearly to each other, and the two hydrophobic chains are attached to adjacent beads at one end of the head region. The chain lengths may be symmetric or asymmetric as shown. Note that there is no bending stiffness within the head region which leads it to assume a compact, globular shape.

contains m hydrophilic beads (see Fig. 1). Based on previous work we have used the following parameter set. The bead self-interactions have the value $a_{ii}=25$ following Groot and Warren,¹⁵ except for the amphiphile head-head, a_{HH} , which we vary to explore its effects on the membrane properties. Our simulations show that if a_{HH} is independent of the lipid tail length, the resulting bilayers have an area stretch modulus that increases strongly with tail length (data not shown). Bilayers whose area stretch modulus is approximately independent of tail length, as found in experiments on lipid vesicles,⁴ are formed if the head-head interaction is proportional to the lipid tail length (see Table I). From Table I, the dependences of a_{HH} on the length of the tail group are described as

$$a_{HH} = 5n_t + 10, \quad (2.6)$$

for amphiphile with three head beads, where n_t is the total number of tail beads in the amphiphile, and

$$a_{HH} = 5n_t + 5, \quad (2.7)$$

for amphiphile with four head beads.

The tail-water, tail-head, and head-water parameters are $a_{TW}d_0/k_B T = 75$, $a_{HT}d_0/k_B T = 50$, and $a_{HW}d_0/k_B T = 35$, respectively, to represent the strong hydrophobic repulsion of the oily chains from the water, their lesser repulsion from the head groups, and the weak hydrophilicity of the head groups. The dissipative force parameter, γ_{ij} , is important for the evolution of the bead coordinates, but as we are interested in equilibrium properties of the membranes we have used the

TABLE I. The dependence of head-group interaction parameter on the length of the tail group.

Amph.	a_{HH} ($k_B T/d_0$)	Amph.	a_{HH} ($k_B T/d_0$)
$H_3(T_6)_2$	40	$H_4(T_6)_2$	35
$H_3(T_7)_2$	45	$H_4(T_7)_2$	40
$H_3(T_8)_2$	50	$H_4(T_8)_2$	45
$H_3T_7T_5$	40	$H_4T_7T_5$	35

values from our previous work²⁰ as they lead to well-formed bilayers. Finally, the Hookean spring parameters and bending stiffness are also taken from the same reference²⁰ and have the values $k_2 d_0^2 / k_B T = 128$, $l_0 / d_0 = 0.5$, and $k_3 / k_B T = 20$, respectively.

Simulations are performed in a cubical box of constant volume $V = (32d_0)^3$ with density $\rho d_0^3 = 3$ beads/unit volume, which gives approximately 100 000 beads of all types. The number of amphiphiles in the bilayer, N , is around 1600 and is determined by the projected area per amphiphile, A_{pr} and the box size. The bilayer is preassembled in the box and the remaining free volume filled with water particles to the desired density. All simulations are carried out at a reduced temperature $T=1$, and we have used the equilibrium area per amphiphile at the bilayer's tensionless state and in-plane diffusion coefficient to extract the length and time scale for the simulations giving $d_0 = 0.7$ nm and $t_0 = 0.46$ ns. Each simulation has 100 000 steps of which the first 50 000 are discarded and observable averages are constructed from at least 1000 independent samples. The equations of motion are integrated using a velocity Verlet scheme⁶ with a step size $dt = 0.02t_0$. By assigning a typical diffusion coefficient for a DMPC lipid bilayer, $5 \mu\text{m}^2/\text{s}$, and using $d_0 = 0.7$ nm, one simulation of 10^5 steps is equivalent to $0.9 \mu\text{s}$ of real time, and requires 80 CPU h on a single-processor Pentium system.

III. RESULTS

We first present results for the bilayer surface tension, area stretch modulus, and bending stiffness, and then look in more detail at the bead density distribution and lateral stress profile through the bilayer.

A. Area stretch modulus of bilayers with symmetric and asymmetric chain lengths

Experiments on lipid bilayer vesicles have found that the area stretch modulus of such vesicles is approximately independent of the lipid tail length, but that the membrane bending stiffness increases with tail length.⁴ Mean-field theories of the dependence of membrane curvature elastic energy on the lipid tail length and head-group area also predict a rise in membrane bending stiffness with tail length.²⁴ In order to compare our simulated membranes with these results we have measured the membrane's area stretch modulus as a function of tail length and effective head-group size.

If we assume a dependence of the surface tension, Σ , on the bilayer projected area, A_{pr} , and amphiphile tail length, n_1 , of the form¹¹

$$\Sigma(A, n_1) \approx K[A_{pr} - A_0(n_1)]/A_0(n_1), \quad (3.1)$$

where A_0 is the projected area at zero surface tension, we can calculate the area stretch modulus, K , of a bilayer formed of amphiphiles with tail length n_1 .

Figure 2 shows the variation of the membrane surface tension for amphiphiles with architecture $H_3(T_{n_1})_2$, where $n_1 = 6, 7, 8$ hydrophobic beads per tail, and for one amphiphile with mismatched tails, $H_3T_7T_5$, that contains the same number of hydrophobic beads in total as the $H_3(T_6)_2$ architecture. The stretch modulus, which is given by the slope of

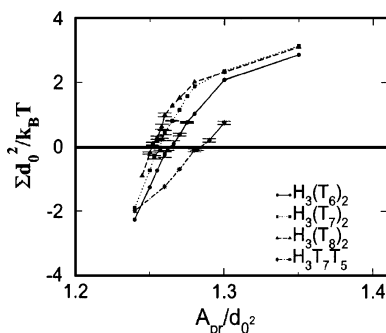


FIG. 2. Variation of the surface tension with the projected area per amphiphile for bilayers composed of $H_3(T_{n_1})_2$ amphiphiles for several tail lengths and $H_3T_7T_5$ amphiphiles. The error bars are only shown for points that are used to calculate the stretch modulus values.

the surface tension at the zero crossing point, is almost independent of the tail length if the H bead's repulsion parameter is increased proportionally to the increase in tail length. The membrane composed of asymmetric-tail amphiphiles has a significantly smaller slope than the other three curves. These results are consistent with the experimental results of Ali *et al.*,⁵ where they find that membranes formed of lipids with mismatched tail lengths are typically much softer to bending modes than the ones formed from lipids with symmetric tails.

In Fig. 2, it is also shown that the projected area decreases slowly with tail length for the symmetric-tail amphiphile which is consistent with experimental results.⁵ Note that a negative surface tension indicates that the bilayer is laterally compressed, although it has not buckled at the projected areas shown as indicated by the surface tension not being independent of area.²⁰

To explore further the relationship between the influence of head-group size and tail length on membrane properties, we have also measured the surface tension for amphiphiles with four hydrophilic beads per head group (Fig. 3). Qualitatively similar results are found as for the amphiphiles containing three beads per head group. However, the curves for symmetric-tail amphiphiles are more tightly clustered than for the smaller head group. The area stretch modulus for the membrane containing asymmetric amphiphiles is again much smaller than the value for symmetric amphiphiles. Our data

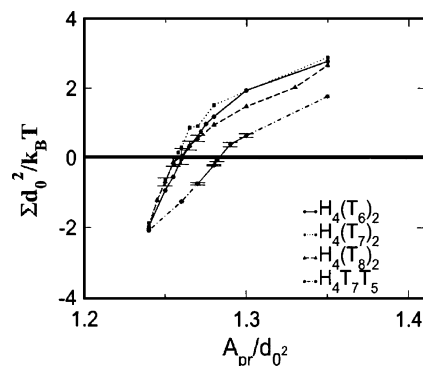


FIG. 3. Variation of the surface tension with the projected area per amphiphile for bilayers composed of $H_4(T_{n_1})_2$ amphiphiles for several tail lengths and $H_4T_7T_5$ amphiphiles. The error bars are only shown for points that are used to calculate the stretch modulus values.

TABLE II. We summarize here our results on membrane area stretch modulus and bending rigidity for the various amphiphile architectures studied, and give information on the equilibrium area per amphiphile and membrane width. The results shown in the table are obtained from averaging over five independent simulations for each projected area. Note that K was calculated using only the points around the tensionless state by taking $k_B T$ at room temperature and $d_0=0.7$ nm.

Amph.	A_0/Nd_0^2	K (dyn/cm)	$\kappa(k_B T)$	ℓ_{me}
$H_3(T_6)_2$	1.262	736 ± 49	84 ± 6	6.79 ± 0.01
$H_3(T_7)_2$	1.257	982 ± 78	149 ± 12	7.85 ± 0.01
$H_3(T_8)_2$	1.252	1186 ± 43	231 ± 8	8.88 ± 0.01
$H_3T_7T_5$	1.282	468 ± 12	52 ± 1	6.68 ± 0.01
$H_4(T_6)_2$	1.26	775 ± 38	96 ± 5	7.1 ± 0.01
$H_4(T_7)_2$	1.257	1011 ± 21	166 ± 3	8.16 ± 0.01
$H_4(T_8)_2$	1.26	486 ± 109	122 ± 23	9.17 ± 0.01
$H_4T_7T_5$	1.282	590 ± 17	58 ± 2	6.97 ± 0.01

show that changing the tail architecture of the amphiphile from symmetric to asymmetric length, while keeping the same total number of tail beads, reduces the area stretch modulus of the bilayer by around 40% (see Table II).

For $H_4(T_8)_2$ amphiphile, with $a_{HH}d_0/k_B T=45$, we found the formation of bilayers with the appearance of an interdigitated structure at some parts of the bilayers (see Fig. 4). This structure is formed because of the strong repulsion between the head groups which increases the head-group surface area and concomitantly create voids in the hydrophobic core. Since voids in the hydrophobic core are energetically unfavorable, the interdigitated phase is formed, where the amphiphile tails from the opposing monolayers interpenetrate to fill the voids. The increment in the water head-group area explains the decreasing of the bilayer area stretch modulus and concomitant the bending modulus, as shown in Table II.

Figure 5 shows the surface tension of a membrane as a function of the projected area per amphiphile for two tail lengths and two head-group sizes: $H_3(T_6)_2$, $H_4(T_6)_2$, $H_3(T_7)_2$, and $H_4(T_7)_2$. The surface tension near its zero crossing does not appear to distinguish between amphiphiles with a larger head group and smaller repulsion (four H beads, $a_{HH}d_0/k_B T=35$) and a smaller head group and larger repulsion (three H beads, $a_{HH}d_0/k_B T=40$). This suggests that it is the *effective* size of the amphiphile head group that influences the bilayer's material properties, and not the exact

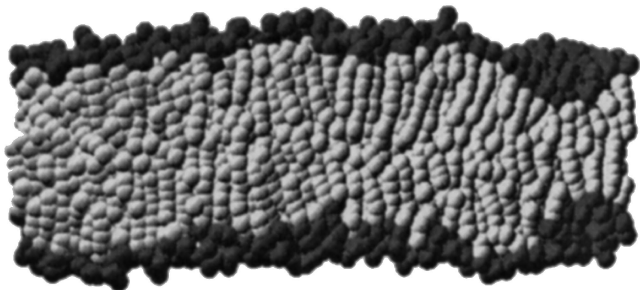


FIG. 4. Snapshot of $H_4(T_8)_2$ bilayer at surface tension $\Sigma d_0^2/k_B T = 0.091 \pm 1.56$ and area per amphiphile $A_{pr}/d_0^2 = 1.265$. Note the interdigitated region at the right side of the image, where the width is smaller than the average.

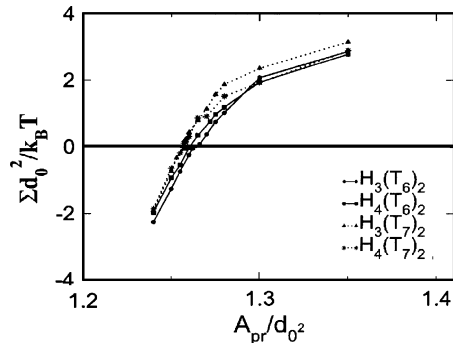


FIG. 5. Variation of the surface tension with the projected area per amphiphile for bilayers composed of $H_3(T_6)_2$, $H_4(T_6)_2$, $H_3(T_7)_2$, and $H_4(T_7)_2$ amphiphiles.

number of hydrophilic beads alone nor the absolute magnitude of the head-head repulsion parameter alone.

Table II shows the numerical results for K , the mean bilayer width ℓ_{me} , and bilayer bending rigidity, κ , which is estimated from the relation¹²

$$\kappa = K \ell_{me}^2 / 48. \quad (3.2)$$

It can be seen that the bilayer width is linear in the amphiphile tail length (see column 5 of Table II). We note here that the amphiphile end-to-end length is also linear in the number of beads per tail (data not shown). The amphiphile architectures shown in Table II exhibit an area per molecule around 62 \AA^2 in the tensionless state, which is quite close to the experimental value of the equilibrium area per molecule of DPPC in a bilayer, around 60 \AA^2 .^{2,25}

B. Effects of chain asymmetry on bilayer density and lateral stress profiles

We have shown in the previous section that a planar bilayer patch composed of a single type of amphiphile with asymmetric chains has a significantly weaker area stretch modulus [and therefore also a weaker bending modulus using Eq. (3.2)] than a bilayer in which the amphiphile chains are symmetric. In this section we show that the chain asymmetry strongly influences the bead distribution within the bilayer and also modifies the lateral stress profile.

The bilayer shown in Fig. 6 contains 1598 $H_4T_7T_5$ amphiphiles and has approximately zero surface tension, $\Sigma d_0^2/k_B T = -0.05 \pm 1.49$ with projected area per amphiphile $A_{pr}/d_0^2 = 1.282$. The projected area per amphiphile for $H_4T_7T_5$ bilayer is slightly larger than the value of $A_{pr}/d_0^2 = 1.26$ for

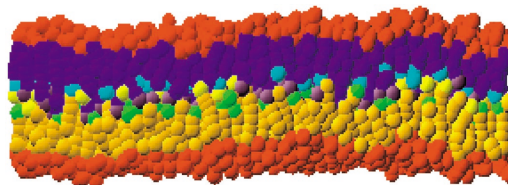


FIG. 6. (Color) Snapshot of a $H_4T_7T_5$ bilayer, where the hydrophobic parts of the two monolayers and each of the last tail beads are colored differently to show the chain interdigitations. The bilayer contains 1598 amphiphiles and has $\Sigma d_0^2/k_B T = -0.05 \pm 1.49$ and $A_{pr}/d_0^2 = 1.282$.

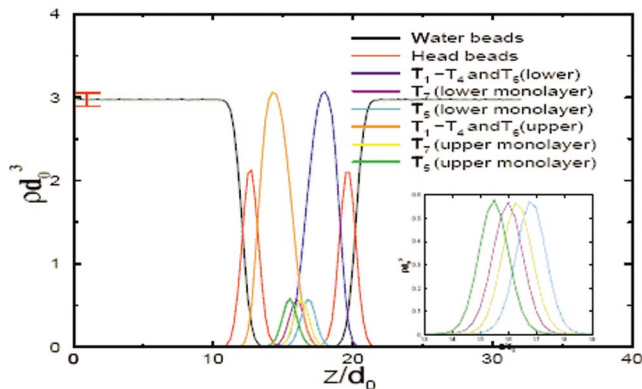


FIG. 7. (Color) Bead number density profiles for $H_4T_7T_5$ bilayer for the tensionless state. One error bar is given in red at $\rho d_0^3 = 2.973 \pm 0.079$. The inset figure shows the enlargement of the last tail beads density profile of each amphiphile.

the relaxed $H_4(T_6)_2$ bilayer. A difference of $A_{pr}/d_0^2 = 0.022$ corresponds to 0.01 nm^2 or 1 \AA^2 . This difference is not experimentally significant.

The lateral density profiles of the hydrophobic and hydrophilic beads in the $H_4T_7T_5$ bilayer, together with the water beads, are shown in Fig. 7. The density profile of the T_7 bead from upper monolayer overlaps with the density profile of the T_7 bead from lower monolayer, indicating that the two monolayers are interdigitated. The density distributions of the terminal beads, T_5 , of the shorter chains show a lesser degree of overlap. Given that the shorter chains of each amphiphile cannot penetrate to the center of the bilayer as much as the longer chains, the overall bead density in the midplane is reduced. The longer chains therefore pack less tightly at the bilayer midplane, so reducing the area stretch modulus.

The amphiphile end-to-end length in the tensionless state of $H_4T_7T_5$ is $\langle \ell_{ee} \rangle / d_0 = 3.51 \pm 0.01$. The bilayer thickness is $\langle \ell_{me} \rangle / d_0 = 6.97 \pm 0.01$, which is only slightly thinner than the value of $\langle \ell_{me} \rangle / d_0 = 7.1 \pm 0.01$ for relaxed $H_4(T_6)_2$ bilayer. From Eq. (3.2) we see that the decreased area stretch modulus results in a smaller bending modulus given that the bilayer thickness is approximately the same.

The lateral stress profile,

$$s(z) \equiv \Sigma_T(z) - \Sigma_N(z), \quad (3.3)$$

is calculated from the difference of the tangential and normal components of the stress tensor summed over all potentials and averaged over thin slices parallel to the bilayer surface. The detail of the stress tensor calculation is described in the work of Goetz and Lipowsky,¹¹ which extends the work of Schofield and Henderson.²⁶ In Fig. 8, we show the lateral stress profiles for bilayers composed of $H_3(T_6)_2$, $H_4(T_6)_2$, and $H_4T_7T_5$ amphiphiles, respectively. The similarity of the profiles for the $H_3(T_6)_2$ and $H_4(T_6)_2$ amphiphiles demonstrates that only the effective head-group interactions influence the bilayer stress distribution, and not the number of hydrophilic beads and their head-head interaction separately. The stress profile for the asymmetric amphiphiles shows a different form from the other two profiles. The inner pairs of positive peaks and negative peaks have shrunk, indicating that the stress near the center of the bilayer has been reduced

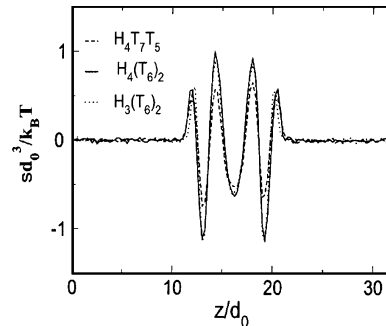


FIG. 8. Stress profiles for $H_4T_7T_5$, $H_4(T_6)_2$, and $H_3(T_6)_2$ bilayers at approximately tensionless state.

for the asymmetric chain case. The outer positive peaks are almost identical for all three cases. These results show that the chain asymmetry strongly modulates the stress distribution near the bilayer midplane without significantly changing either the bilayer width or the interactions at the water-bilayer interface.

IV. CONCLUSIONS

Dissipative particle dynamics simulations have been used to systematically and quantitatively measure the area stretch modulus and bending modulus for bilayers composed of a homologous series of amphiphiles and compared their properties to experimental lipid bilayer membranes. We have used DPD rather than coarse-grained MD simulations, as it can be applied to significantly larger systems while consuming orders-of-magnitude less computer time. For membrane properties that are averages over many hundreds of molecules, such as the bead density profiles, lateral stress profiles, and material properties studied here, DPD has been found to produce results comparable to coarse-grained MD simulations.²⁰

Experimental results on the independence of lipid bilayer membrane area stretch modulus on lipid tail length are reproduced if the effective head-head repulsion parameter is proportional to the amphiphile tail length. Although the area stretch modulus is less dependent on tail length than for simulated membranes of single-tail amphiphiles,²⁰ there is a residual increase with tail length and concomitant reduction in preferred area. The latter result is consistent with experimental data of Ali *et al.*⁵ and Petrache *et al.*²⁷ The results of Rawicz *et al.*⁴ on lipid bilayer vesicles that their area stretch modulus is almost independent of lipid tail length are thus only partially reproduced, but the increase of the bilayer bending modulus with increasing tail length is well reproduced.

We have simulated membranes composed of double-tailed amphiphiles with the same total numbers of tail beads as in the symmetric ones but with asymmetric tail lengths. Interdigitation of the terminal hydrophobic beads of the amphiphiles is found in the simulations. Additionally, the extra free space available to the longer chains near the bilayer midplane significantly weakens the bilayer compared to those composed of symmetric-tail amphiphiles. Such a de-

crease in the area stretch modulus of bilayers composed of asymmetric amphiphiles has been found in the experimental work by Ali *et al.*⁵

In a separate study, we have found that the inclusion of amphiphiles with short tails into a bilayer composed of amphiphiles with long tails has a similar effect on reducing the stretch modulus and bending modulus as that of the pure system composed of asymmetric tails.²⁸ Further, the thickness of bilayers composed of asymmetric chains is very close to that of bilayers composed of symmetric chains, which is in agreement with the experimental results of Hui *et al.*²⁹ for C(18):C(10)PC membranes in comparison with the thickness of C(14):C(14)PC membranes calculated by Janiak *et al.*³⁰ The thickness of $H_3(T_6)_2$ bilayer obtained from simulation is $\langle \ell_{me} \rangle = 4.75$ nm which is comparable with the width of typical 18-carbon diacyl lipid bilayer, 4 nm.⁴

Finally, we also find that amphiphiles with asymmetric chains significantly modify the stress distribution near the bilayer midplane while leaving the water-hydrophobic interfacial stress almost unchanged. Such depth-dependent redistribution of stress has been suggested as a possible mechanism by which anaesthetics work,²³ and membrane-bound proteins, such as mechanosensitive channels.³¹ We believe that DPD simulations can be used to explore systematically, and in a quantitative manner, the properties of the complex fluid environment that are crucial for the function of membrane-bound proteins.

¹B. Alberts, D. Bray, J. Lewis, M. Raff, K. Roberts, and J. D. Watson, *Molecular Biology of the Cell*, 2nd ed. (Garland, New York, 1989).

²D. D. Lasic, in *Vesicles*, Surfactant Science Series Vol. 62, edited by M. Rosoff (Marcel Dekker, Inc., New York, 1996).

³D. Needham and R. M. Hochmuth, *Biophys. J.* **55**, 1001 (1989).

⁴W. Rawicz, K. C. Olbrich, T. McIntosh, D. Needham, and E. Evans, *Biophys. J.* **79**, 328 (2000).

⁵S. Ali, J. M. Smaby, M. M. Momsen, H. L. Brockman, and R. E. Brown, *Biophys. J.* **74**, 338 (1998).

⁶M. P. Allen and D. J. Tildesley, *Computer Simulation of Liquids* (Clarendon, Oxford, 1987).

⁷S. Ohta-lino, M. Pasenkiewicz-Gierula, Y. Takaoda, H. Miyagawa, K. Kitamura, and A. Kusumi, *Biophys. J.* **81**, 217 (2001).

⁸E. Lindahl and O. Edholm, *Biophys. J.* **79**, 426 (2000).

⁹S. O. Nielsen, C. F. Lopez, G. Srinivas, and M. L. Klein, *J. Phys. Chem. B* **108**, 8153 (2004).

¹⁰S. J. Marrink, E. Lindahl, O. Edholm, and A. E. Mark, *J. Am. Chem. Soc.* **123**, 8638 (2001).

¹¹R. Goetz and R. Lipowsky, *J. Chem. Phys.* **108**, 7397 (1998).

¹²R. Goetz, G. Gompper, and R. Lipowsky, *Phys. Rev. Lett.* **82**, 221 (1999).

¹³S. J. Marrink and A. E. Mark, *J. Am. Chem. Soc.* **125**, 11144 (2003).

¹⁴P. J. Hoogerbrugge and J. M. V. A. Koelman, *Europhys. Lett.* **19**, 155 (1992).

¹⁵R. D. Groot and P. B. Warren, *J. Chem. Phys.* **107**, 4423 (1997).

¹⁶R. D. Groot and K. L. Rabone, *Biophys. J.* **81**, 725 (2001).

¹⁷S. Yamamoto, Y. Maruyama, and S. Hyodo, *J. Chem. Phys.* **116**, 5842 (2002).

¹⁸M. Laradji and P. B. Sunil Kumar, *Phys. Rev. Lett.* **93**, 198105 (2004).

¹⁹S. Yamamoto and S. Hyodo, *J. Chem. Phys.* **118**, 7937 (2003).

²⁰J. C. Shillcock and R. Lipowsky, *J. Chem. Phys.* **117**, 5048 (2002).

²¹M. Kranenburg, M. Venturoli, and B. Smit, *Phys. Rev. E* **67**, 060901 (2003).

²²L. Rekvig, M. Kranenburg, J. Vreede, B. Hafskjold, and B. Smit, *Langmuir* **19**, 8195 (2003).

²³R. S. Cantor, *Biophys. J.* **76**, 2625 (1999).

²⁴I. Szleifer, D. Kramer, A. Ben-Shaul, D. Roux, and W. M. Gelbart, *Phys. Rev. Lett.* **60**, 19 (1988).

²⁵J. F. Nagle, R. T. Zhang, S. Tristram-Nagle, W. J. Sun, H. I. Petrache, and R. M. Suter, *Biophys. J.* **70**, 1419 (1996).

²⁶P. Schofield and J. R. Henderson, *Proc. R. Soc. London, Ser. A* **379**, 231 (1982).

²⁷H. I. Petrache, S. W. Dodd, and M. F. Brown, *Biophys. J.* **79**, 3172 (2000).

²⁸G. Illya, Ph.D. thesis, University of Potsdam, 2004.

²⁹S. W. Hui, J. T. Mason, and C.-H. Huang, *Biochemistry* **23**, 5570 (1984).

³⁰M. J. Janiak, D. M. Small, and G. G. Shipley, *Biochemistry* **15**, 4575 (1976).

³¹J. Gullingsrud and K. Schulten, *Biophys. J.* **85**, 2087 (2003).